Triggered single photons from a quantum dot

Charles Santori, Matthew Pelton, Glenn Solomon^{*}, Yseulte Dale, and Yoshihisa Yamamoto[†]

Quantum Entanglement Project, ICORP, JST, E.L. Ginzton Laboratory, Stanford University, Stanford, California 94305

(Submitted to Phys. Rev. Lett. on October 9, 2000)

We demonstrate a new method for generating triggered single photons. After a laser pulse generates excitons inside of a single quantum dot, electrostatic interactions between them and the resulting spectral shifts allow a single emitted photon to be isolated. Autocorrelation measurements show a reduction of the two-photon probability to 0.12 times the value for Poisson light. Strong antibunching persists when the emission is saturated. The emitted photons are also polarized.

PACS numbers: 42.50.Dv, 78.66.-w, 73.23.-b

Photons from classical light sources, which usually consist of a macroscopic number of emitters, follow Poisson statistics or super-Poisson statistics [1]. With a single quantum emitter, however, one can hope to generate a regulated photon stream, containing one and only one photon in a given time interval. Such an "anti-bunched" source would be useful in the new field of quantum cryptography, where security from eavesdropping depends on the ability to produce no more than one photon at a time [2,3].

Continuous streams of anti-bunched photons were first observed from single atoms and ions in traps [4,5]. More recently, experiments demonstrating triggered single photons have used single molecules as the emitters, excited optically either by laser pulses [6,7] or through adiabatic following [8].

Solid-state sources have potential advantages. Most importantly, they may be conveniently integrated into larger structures, such as distributed-Bragg-reflector (DBR) microcavities [9,10] to make monolithic devices. In addition, most do not suffer from the photo-bleaching effect that severely limits the lifespan of many molecules. The first experimental effort towards a solid-state singlephoton source was based on electrostatic repulsion of single carriers in a semiconductor micropost p-i-n structure [11]. Milli-Kelvin temperatures were required, however, and sufficient collection efficiency to measure the photon autocorrelation function was not obtained. More recently, continuous anti-bunched fluorescence has been seen from color centers in a diamond crystal [12,13] and from CdSe quantum dots [14].

Our method to generate triggered single photons involves pulsed optical excitation of a single quantum dot and spectral filtering to remove all but the last emitted photon. Optically active quantum dots confine electrons and holes to small regions so that their energy levels are quantized [15]. If several electrons or holes are placed in the dot at the same time, they will, to a first approximation, occupy single-particle states as allowed by the Pauli exclusion principle. However, electrostatic interactions between the particles cause perturbations in the eigenstates and energies. For example, if two electronhole pairs (excitons) are created (a "biexcitonic" state), the first pair to recombine emits at a slightly lower energy than the second pair, due to a net attractive interaction [16,17]. We exploit this effect to generate single photons not only through regulated absorption, as in the single-molecule experiments, but also through this emission property, that the last photon to be emitted after an excitation pulse has a unique wavelength, and therefore can be spectrally separated from the others.

A sample was fabricated containing self-assembled InAs quantum dots surrounded by a GaAs matrix [15]. The dots were grown by molecular beam epitaxy (Fig. 1a) at a high temperature to allow alloying with the surrounding GaAs, thereby shortening the emission wavelength. They were then capped by 75 nm of GaAs. Mesas about 120 nm tall, 200 nm wide, and spaced 50 μ m apart were fabricated by electron-beam lithography and dry etching. The dots are sparse enough (11 μ m⁻²) that the smallest mesas contain, on average, fewer than one dot.

The experimental setup is shown in Fig. 1b. The sample was cooled to 5K in a cryostat and placed close to the window. A mode-locked Ti-sapphire laser with 2.9 ps pulses and a 76 MHz repetition rate was focused onto a mesa from a steep $(53.5^{\circ} \text{ from normal})$ angle, down to an 18 μ m effective spot diameter. Emission from the dot inside the mesa was collected with an NA=0.5 aspheric lens, and focused onto a pinhole that effectively selected a 5 μ m region of the sample for collection. A rotatable half-wave plate followed by a horizontal polarizer selected a particular linear polarization. The light was then sent to a CCD camera, a spectrometer, or a Hanbury Brown-Twiss configuration for measuring the photon autocorrelation function. Two EG&G "SPCM" photon counters were used for detection, with efficiencies of 40% at 877 nm, and 0.2 mm-wide active areas. A monochrometer-type configuration defined a 2 nm-wide measurement bandwidth, with the center wavelength determined by the detector position. Additional rejection of unwanted light (scattered pump light and stray room light) was obtained with a 10 nm bandpass filter attached

to each detector. The electronic pulses from the photon counters were used as start (t_1) and stop (t_2) signals for a time interval counter, which recorded these intervals $\tau = t_2 - t_1$ as a histogram.

Mesas containing single dots were identified by their optical emission spectra. The mesa chosen for this experiment contains a dot whose main ground-state emission wavelength is 876.4 nm. With continuous-wave (CW) excitation above the GaAs bandgap, the emission spectrum (Fig. 1c, left) displays several lines, as has been reported elsewhere [18]. We believe that these lines all come from a single dot because another mesa shows a nearly identical emission pattern (peak heights, spacings and widths), except for an overall wavelength shift, suggesting that this pattern is not random. To avoid ionization of the dot or delayed capture of electrons and holes, we tuned the laser wavelength to an absorption resonance at 857.5 nm, thus creating excitons directly inside of the dot. With resonant excitation, emission peaks 3 and 4 almost disappear (Fig. 1c, right), and therefore we believe that they represent emission from other charge states of the dot [19]. We identify peak 1 as ground-state emission after the capture of a single exciton, and peak 2 as "biexcitonic" emission after the capture of two excitons. This assignment is supported by the dependence of the emission line intensities on pump power (Fig. 2a), showing linear growth of peak 1 and quadratic growth of peak 2 in the weak pump limit. A biexcitonic energy shift of 1.7 meV is seen.

Under pulsed, resonant excitation, a clear saturation behavior is seen for peak 1 (Fig. 2b). Although peak 2 and its surrounding peaks (presumably multipleexcitonic emission) continue to grow as the pump power is increased, peak 1 reaches a maximum value, since only the last exciton to recombine emits at this particular wavelength. This is shown quantitatively in Fig. 2c. Here, a photon counter was used to measure the emission rate versus pump power, with the detection band tuned to accept peak 1 but reject peak 2 (see dashed line, Fig. 1c). A simple saturation function for unregulated absorption that fits the data well is

$$I = I_0 (1 - e^{-P/P_{sat}}), \qquad (1)$$

where I is the measured intensity for single-exciton emission, P is the pump power, and I_0 and P_{sat} are fitting parameters that characterize the total collection efficiency and the absorption rate, respectively.

The emission from peak 1 was also linearly polarized. Since the degree of polarization of the emission depended strongly on the pump polarization angle, we believe that the effect is largely due to the selection rules for photon absorption and emission [20,21]. The polarization of a pump photon is transferred into the spin of an exciton, and if no spin relaxation occurs, the spin is transfered back to the emitted photon polarization. The polarization is linear, as would be expected for asymmetric dots under no magnetic field [22,23]. At the optimal pump polarization used in this experiment, emission polarization with up to 72% visibility was observed at weak pump (Fig. 2d). The lack of perfect visibility was perhaps due to spin relaxation, imperfect selection rules, or effects of the post geometry. The visibility was partially degraded when the pump power was increased into the saturation regime.

We next examine the second-order coherence function, $g^{(2)}(\tau)$, which contains information on photon emission statistics [1]. For a pulsed source, $g^{(2)}(\tau)$ becomes a series of peaks separated by the laser repetition period, and the areas of these peaks give information on photon number correlations between pulses separated by time τ . Of special interest is the central peak at $\tau = 0$, which gives an upper bound on the probability that two or more photons are emitted from the same pulse:

$$2P(n_j \ge 2)/\langle n \rangle^2 \le \frac{1}{T} \int_{-\epsilon}^{\epsilon} g^{(2)}(\tau) d\tau , \qquad (2)$$

where n_j is the number of photons in pulse j, ϵ is chosen to include the entire central peak in the integration region, and T is the pulse repetition period. This result, along with $g^{(2)}(\tau)$, is independent of the collection and detection efficiencies. For a "classical" (Poisson) source, the normalized central peak area (right-hand side of Eq. 2) is one.

Histograms of the time interval $\tau = t_2 - t_1$ taken at four different pump powers are shown in Fig. 3. In the limit of low collection and detection efficiency (≈ 0.0003 combined in our case), these histograms, after correct normalization, approximate the autocorrelation function. The peaks are broader than the limit imposed by the photon counter timing resolution (0.3 ns), and indicate a lifetime for the single-exciton state of about 0.7 ns. The $\tau = 0$ peak shows a large reduction in area, indicating strong anti-bunching. The numbers printed above the peaks indicate the peak areas, properly normalized by dividing the histogram areas by both singles rates. the laser repetition period, and the measurement time. For the numbers shown, the only background counts subtracted were those due to the known dark count rates of the photon counters $(130 \text{ s}^{-1} \text{ and } 180 \text{ s}^{-1})$, almost negligible compared to the singles rates, 19800 s^{-1} and $14000 \,\mathrm{s}^{-1}$ for the two counters at 0.88 mW pump power. When only counts within 2.8 ns of $\tau = 0$ were included, a normalized $q^{(2)}(\tau = 0)$ peak area of 0.12 was obtained at 0.88 mW. Subtracting the constant background floor seen in the data gave an even lower value of 0.095.

The observed anti-bunching has two causes. The first cause is a suppression of the probability for the dot to absorb a second photon after the first photon has been absorbed. If one collects emission from both the single-exciton and multi-exciton lines, the $g^{(2)}(\tau = 0)$ peak area is still reduced to about 0.32 due to limited absorption. A

possible explanation for reduced absorption of the second photon is that electrostatic interactions, similar to those responsible for the 1.7 meV biexcitonic energy shift, move the absorption resonance to a lower energy for the second photon [24]. The second cause for the observed antibunching is that, even if more that one exciton is created, only the last exciton to recombine emits at our collection wavelength. Under these collection conditions, we see a fair degree of anti-bunching at all pump wavelengths, even above band, if the pump power is not too high. The remaining counts seen at $\tau = 0$ under optimal pump and collection conditions are most likely due to imperfect filtering to reject multi-excitonic emission.

While the central autocorrelation peak area is reduced, the adjacent peaks have normalized areas larger than one. This indicates positive correlations between the detected photon numbers from adjacent pulses. This longer-term bunching behavior is better seen in Fig.4, which plots normalized autocorrelation peak areas versus peak number over a longer time span. The extra peak area above one is seen to decay exponentially away from $\tau = 0$. For larger pump powers, the time scale and the magnitude of the effect decrease. A simple model to describe this behavior assumes that the dot randomly "blinks" between two conditions, a fully functioning condition and a "dark" (or wavelength-shifted) condition in which photons are not observed, with time constants τ_{on} and τ_{off} . This model results in

$$h_{m\neq 0} = 1 + \frac{\tau_{off}}{\tau_{on}} e^{-(1/\tau_{off} + 1/\tau_{on})|mT|}, \qquad (3)$$

where h_m is the *m*-th normalized autocorrelation peak area, and T is the laser repetition period. Fitting this model to the data gives the values for τ_{on} and τ_{off} shown on the plots, which are on the order of 100 ns. Longterm (> 1s) blinking behavior has already been reported in strain-induced GaAs dots [25] and InP dots [26], and emission wavelength fluctuations have been reported for InGaAs dots [27]. These effects have been attributed to nearby defects [26] and trapped charges [27]. The more rapid blinking behavior seen here is unwanted and necessarily decreases the efficiency of the device, but it should be contrasted with the bleaching behavior of single molecules. The quantum dot described here has been studied for months and cooled down to 5K about 30 times without ceasing to function or changing significantly.

The internal efficiency of single-photon generation is difficult to determine because the collection efficiency of the first lens depends on uncertain factors such as the position of the dot within the mesa and the quality of the surface. An upper limit of 0.57 at 2.63 mW assumes that once the emission is saturated, the only reductions are due to imperfect polarization and the ≈ 100 ns blinking behavior described above. This would imply a collection efficiency through the first lens of 0.006. To improve the collection efficiency, a realistic solution is to place the dot inside of a DBR microcavity to direct most of the spontaneous emission into a single mode [9,10].

In summary, we have demonstrated a new method for generating triggered single photons, using a single quantum dot excited on resonance by laser pulses. The method takes advantage of Coulomb interactions between excitons and the resulting spectral shifts to isolate single emitted photons. We observed a ten-fold two-photon probability suppression and strongly polarized emission, suggesting that a single quantum dot is a promising candidate for a practical single-photon source, although some unwanted blinking was also observed. The main remaining challenge is to improve the collection efficiency, which we expect can be accomplished by growing a microcavity around the dot.

We thank S. Somani for loaning critical equipment. Financial assistance for C. M. S. was provided by the National Science Foundation. Financial assistance for C. M. S. and M. P. was provided by Stanford University.

- * Also at Solid State Photonics Laboratory, Stanford.
- [†] Also at NTT Basic Research Laboratories, Atsugishi, Kanagawa, Japan.
- D. F. Walls and G. J. Milburn, *Quantum Optics* (Springer-Verlag, Berlin, 1994).
- [2] G. Brassard, N. Lütkenhaus, T. Mor, and B. Sanders, *Phys. Rev. Lett.* 85, 1330 (2000).
- [3] G. Brassard and C. Crépeau, Sigact News 27, 13 (1996).
- [4] H. J. Kimble, M. Dagenais, and L. Mandel, *Phys. Rev. Lett.* **39**, 691 (1977).
- [5] F. Diedrich and H. Walther, Phys. Rev. Lett. 58, 203 (1987).
- [6] F. De Martini, G. Di Giuseppe, and M. Marrocco, *Phys. Rev. Lett.* **76**, 900 (1996).
- [7] B. Lounis and W.E. Moerner, *Nature* **407**, 491 (2000).
- [8] C. Brunel, B. Lounis, P. Tamarat, and M. Orrit, *Phys. Rev. Lett.* 83, 2722 (1999).
- [9] B. Ohnesorge et al., Phys. Rev. B, 56. R4367 (1997).
- [10] J. M. Gérard et al., Phys. Rev. Lett., 81, 1110 (1998).
- [11] J. Kim, O. Benson, H. Kan, and Y. Yamamoto, *Nature* 397, 500 (1999).
- [12] C. Kurtsiefer, S. Mayer, P. Zarda, and H. Weinfurter, *Phys. Rev. Lett.* 85, 290 (2000).
- [13] R. Brouri, A. Beveratos, J.-P. Poizat, and P. Grangier, *Opt. Lett.* 25, 1294 (2000).
- [14] P. Michler et al., Nature, 406, 968 (2000).
- [15] D. Bimberg et al., Quantum Dot Heterostructures (John Wiley & Sons, Chichester, 1999). For MBE growth of InAs self-assembled dots, see chap. 4.2.
- [16] A. Kuther et al., Phys. Rev. B 58, R7508 (1998).
- [17] M. Bayer, O. Stern, P. Hawrylak, S. Fafard, and A. Forchel, *Nature* **405**, 923 (2000).
- [18] L. Landin, M. S. Miller, M.-E. Pistol, C. E. Pryor, and L. Samuelson, *Science* 280, 262 (1998).

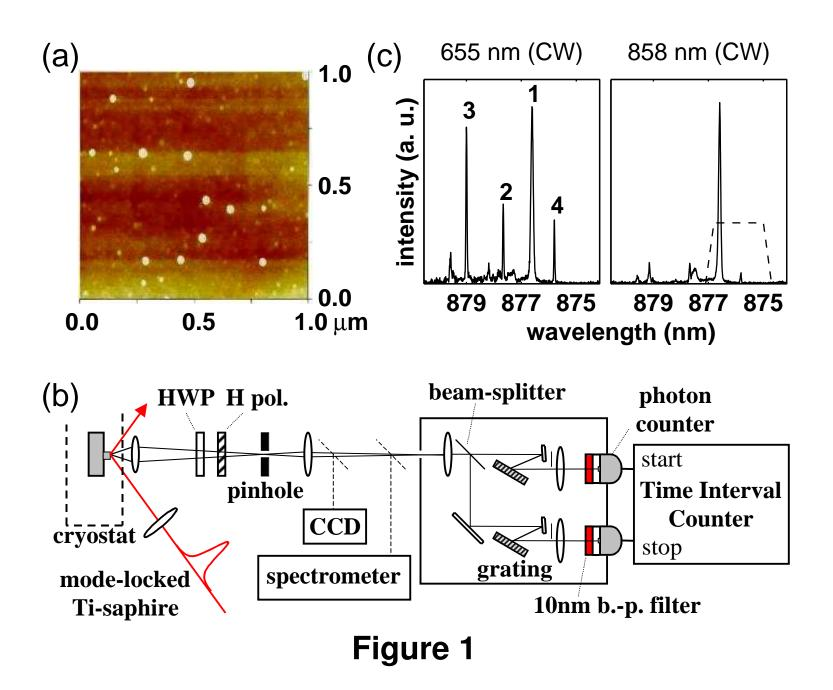
- [19] R. J. Warburton et al., Nature 405, 926 (2000).
- [20] Y. Toda, S. Shinomori, K. Suzuki, and Y. Arakawa, *Phys. Rev. B* 58, R10147 (1998).
- [21] H. Gotoh, H. Ando, H. Kamada, A. Chavez-Pirson, and J. Temmyo, *Appl. Phys. Lett.* **72**, 1341 (1998).
- [22] D. Gammon, E. S. Snow, B. V. Shanabrook, D. S. Katzer, and D. Park, *Phys. Rev. Lett.* **76**, 3005 (1996).
- [23] M. Sugisaki et al., Phys. Rev. B 59, R5300 (1999).
- [24] This is consistent with our observation that, if the pump wavelength is tuned 1.7 meV below the first-photon resonance, strong photon bunching $(g^2(0)$ enhancement factor of about 3.5) occurs. In this case, the energy shift brings the second-photon absorption closer to resonance.
- [25] D. Bertram, M. C. Hanna, and A. J. Nozik, *Appl. Phys. Lett.* 74, 2666 (1999).
- [26] M.-E. Pistol, P. Castrillo, D. Hessman, J. A. Prieto, and L. Samuelson, *Phys. Rev. B* 59 10725 (1999).
- [27] H. D. Robinson and B. B. Goldberg, *Phys. Rev. B* 61, R5086 (2000).

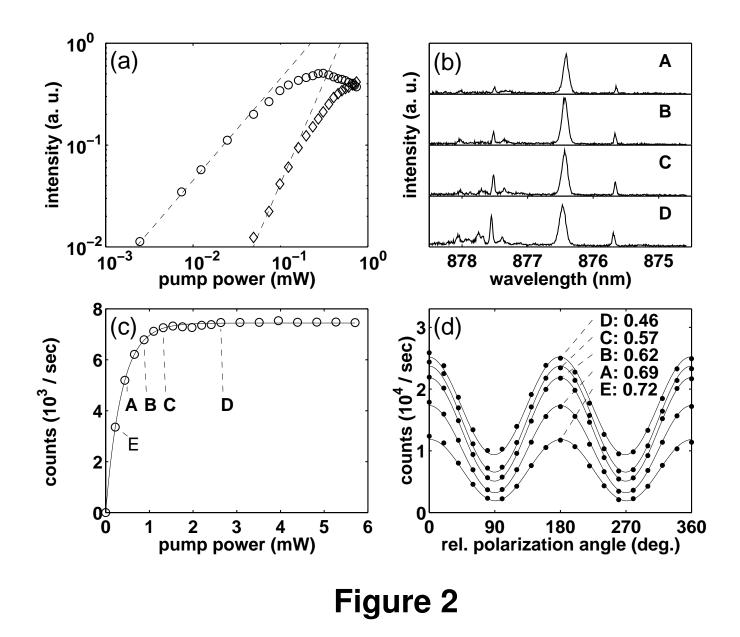
FIG. 1. (a) Atomic force microscope image of uncovered InGaAs self-assembled quantum dots, grown under identical conditions to those used in this experiment. (b) The experimental setup, showing the laser-excited sample (left), collection optics (middle-left), and Hanbury Brown-Twiss configuration (right). (c) Emission spectra from a quantum dot under above-band excitation (left) and resonant excitation (right). The dotted line indicates approximately the portion of the spectrum that reaches the photon counters after filtering.

FIG. 2. (a) A log-log plot of emission line intensity versus above-band (CW) pump power, showing linear growth of peak 1 (circles) and quadratic growth of peak 2 (diamonds). (b) Emission spectra, (c) emission intensity (measured under the filtering condition depicted in Fig.1b), and (d) emission polarization dependence of the dot under pulsed, resonant excitation with powers E,A-D: 0.22 mW, 0.44 mW, 0.88 mW, 1.32 mW and 2.63 mW, respectively. The count rates in (c) are further reduced by an additional bandpass filter. The solid line in (c) is a least-squares fit of Eq. 1, while the solid lines in (d) fit a sinusoid plus an offset, resulting in the shown visibilities (max.-min.)/(max.+min.).

FIG. 3. Histograms of the time intervals $\tau = t_2 - t_1$ between photons detected by the "start" and "stop" counters, for four different excitation powers: (a) 0.44 mW, (b) 0.88 mW, (c) 1.32 mW and (d) 2.63 mW. The numbers printed above the peaks give the normalized autocorrelation peak areas, calculated using a 5.6 ns-wide integration window. The reduction of the $\tau = 0$ peak demonstrates anti-bunching.

FIG. 4. Normalized autocorrelation peak areas (13 ns-wide integration window) obtained from longer time-scale histograms, plotted against peak number, counted from $\tau = 0$, for four different excitation powers: (a) 0.44 mW, (b) 0.88 mW, (c) 1.32 mW and (d) 2.63 mW. The lines are least-squares fits using Eq. 3, and the fitting parameters obtained are shown.





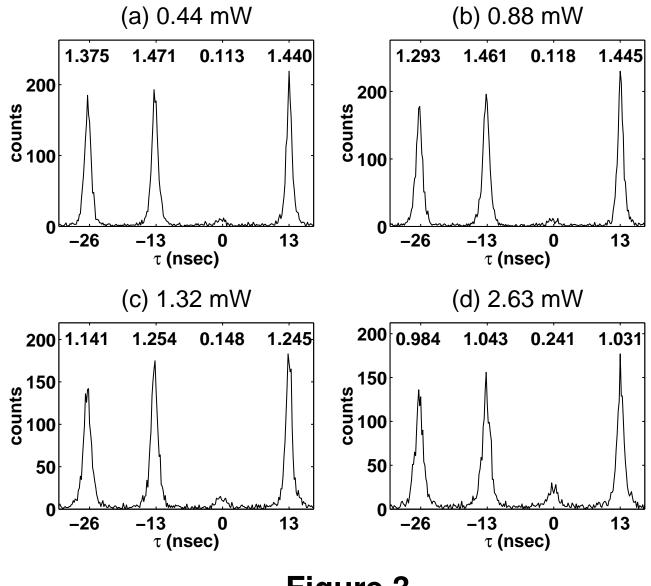


Figure 3

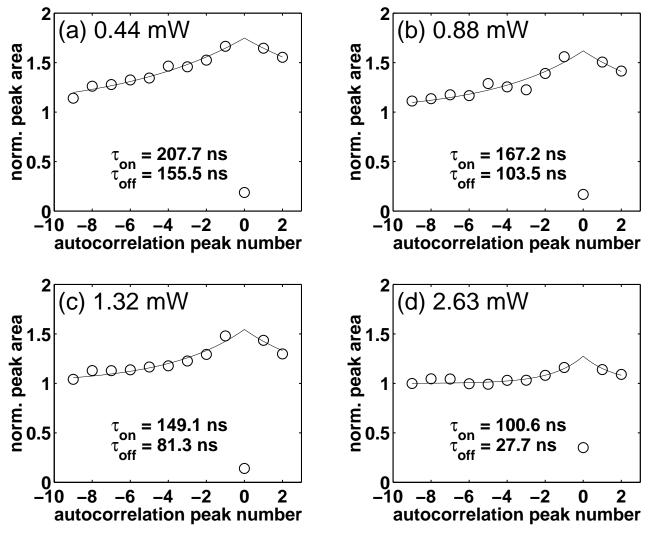


Figure 4